Pure and Applied Geophysics

CrossMark

Analysis of the Far-Field Co-seismic and Post-seismic Responses Caused by the 2011 M_W 9.0 Tohoku-Oki Earthquake

Zhigang Shao,[1] Wei Zhan,[2] Langping Zhang,[1] and Jing Xu[3]

Abstract—We analyzed the far-field co-seismic response of the M_W 9.0 Tohoku-Oki earthquake, which occurred on March 11th 2011 at the Japan Trench plate boundary. Our analysis indicates that the far-field co-seismic displacement was very sensitive to the magnitude of this event, and that a significant co-seismic surface displacement from earthquakes in the Japan Trench region can be observed in Eurasia only for events of $M_W \geq 8.0$. We also analyzed the temporal characteristics of the near-field post-seismic deformation caused by the afterslip and the viscoelastic relaxation following the Japan earthquake. Next, we performed a simulation to analyze the influence of the two post-seismic effects previously mentioned on the far-field post-seismic crustal deformation. The simulation results help explain the post-seismic crustal deformation observed on the Chinese mainland 1.5 years after the event. Fitting results revealed that after the M_W 9.0 Tohoku-Oki earthquake, the afterslip decayed exponentially, and may eventually disappear after 4 years. The far-field post-seismic displacement in Eurasia caused by the viscoelastic relaxation following this earthquake will reach the same magnitude as the co-seismic displacement in approximately 10 years. In addition, the co- and post-seismic Coulomb stress on several NE-trending faults in the northeastern and northern regions of the Chinese mainland were significantly enhanced because of the M_W 9.0 earthquake, especially on the Yilan-Yitong and the Dunhua-Mishan faults (the northern section of the Tan-Lu fault zone) as well as the Yalujiang and the Fuyu-Zhaodong faults.

Key words: The 2011 9.0 Tohoku (Japan) earthquake, Far-field response, Afterslip, Viscoelastic relaxation, Coulomb stress.

1. Introduction

On March 11th, 2011, the M_W 9.0 Tohoku-Oki earthquake ruptured the plate boundary northeast of Japan. This earthquake was the largest earthquake in Japan on record (Tajima *et al.* 2013), and was one of the largest events ever recorded on our planet with modern instrumentation. Intense crustal deformations in the near-field region were detected by the on-shore GPS Earth Observation Network (GEONET) (Ozawa *et al.* 2012; Sato *et al.* 2011) and an off-shore GPS/acoustic system. The maximum co-seismic horizontal displacement recorded by the two observation systems were 5.2 and 31.5 m (Kido *et al.* 2011), respectively. Moreover, co-seismic displacements were clearly detected by far-field GPS receivers located 1000–2000 km away on the Chinese mainland and the Korean Peninsula (Fig. 1, Pollitz *et al.* 2011; Shestakov *et al.* 2012). The maximum co-seismic horizontal displacements observed in China and Korea were up to 35 and 57.7 mm, respectively (Wang *et al.* 2011; Zhao *et al.* 2012; Hwang *et al.* 2012). Shestakov et al. (2012) defined the moment magnitude of this earthquake as 8.8 based on far-field co-seismic GPS data.

The current tectonics of the Japanese Islands can be explained as the interaction between the Pacific, Eurasia, North American, and Philippine Sea plates (Kanamori 1977; Taira 2001). Therefore, plate tectogenesis in the Japanese Islands is very strongly influenced by active volcanoes and earthquakes; the latter are caused by the subduction of the Pacific Plate below the Eurasia Plate at a rate of 8–9 cm/a west of the Japan Trench (Chen *et al.* 2004). The focal depth gradually deepens to 600–700 km from the trench region westward to northeastern China, and both

[1] Key Laboratory of Earthquake Prediction, Institute of Earthquake Science, China Earthquake Administration, Beijing 100036, China.
[2] First Crust Monitoring and Application Center, China Earthquake Administration, Tianjin 300180, China.
[3] Second Crust Monitoring and Application Center, China Earthquake Administration, Xi'an 710054, China. E-mail: xjinggis@163.com
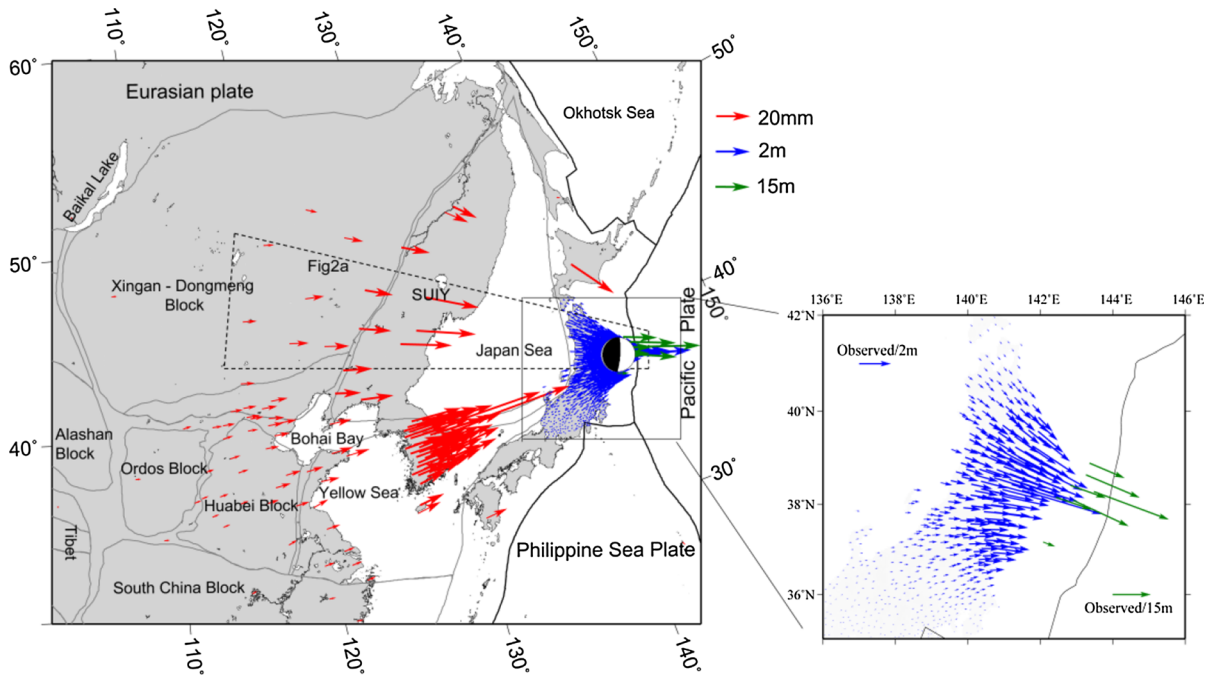
Figure 1

Spatial distribution of the co-seismic displacements caused by the 9.0 Tohoku-Oki earthquake (KIDO *et al.* 2011; INUMA *et al.* 2012). The *green arrows* represent the seabed surface co-seismic displacements, the *blue arrows* are the near-field surface co-seismic displacements on the Japanese Island (GEONET), and the *red arrows* show the far-field co-seismic displacements (WANG *et al.* 2011; ZHAO *et al.* 2012; HWANG *et al.* 2012). The *inlet figure* represents the detailed *arrows* of Japan GPS vectors and sea-bed vectors

shallow and deep high-magnitude earthquakes are very active in this area (DEPARTMENT OF MONITORING and PREDICTION, CHINA EARTHQUAKE ADMINISTRATION 2007; KANAMORI *et al.* 2006). Co- and post-seismic crustal deformation observed on the Chinese mainland after the 9.0 Tohoku-Oki earthquake provided significant data for the analysis of the far-field effects. In this article, we discuss the far-field co- and post-seismic effects using a theoretical simulation.

2. Co-seismic Far-Field Effects of the 9.0 Tohoku-Oki Earthquake

Figure 2 shows the relationship between the co-seismic displacements and epicentral distance for a north-western profile (see the location of the profile in Fig. 1). The figure shows that the co-seismic displacement exponentially decayed with distance from the epicenter (Fig. 2a). This exponential decay of the co-seismic displacements was observed in both the

near-field measurements (collected within the Japanese islands) and the far-field data recorded in eastern China and on the Korean peninsula. The data set collected for the near-field displacements was relatively large and of high quality, and the fitted attenuation index $1/b$ of the near-field co-seismic displacement data agree well with that of the entire profile (Fig. 2b). However, the fitted attenuation index for the far-field co-seismic displacement data, especially more than 1000 km away from the epicenter, is significantly smaller than the profile as a whole (Fig. 2c).

A variety of data were recorded during the M_W 9.0 Tohoku-Oki earthquake, including digital seismic waveforms, continuous GPS data, strong motion seismographs, submarine sonar-GPS integrated data, sea-floor pressure data, InSAR, and tsunami data. Based on these data, the co-seismic dislocation of the 9.0 earthquake can be obtained by several different inversion methods (see, for example, HAYES 2011; SIMONS *et al.* 2011; LAY *et al.* 2011; KOPER *et al.*
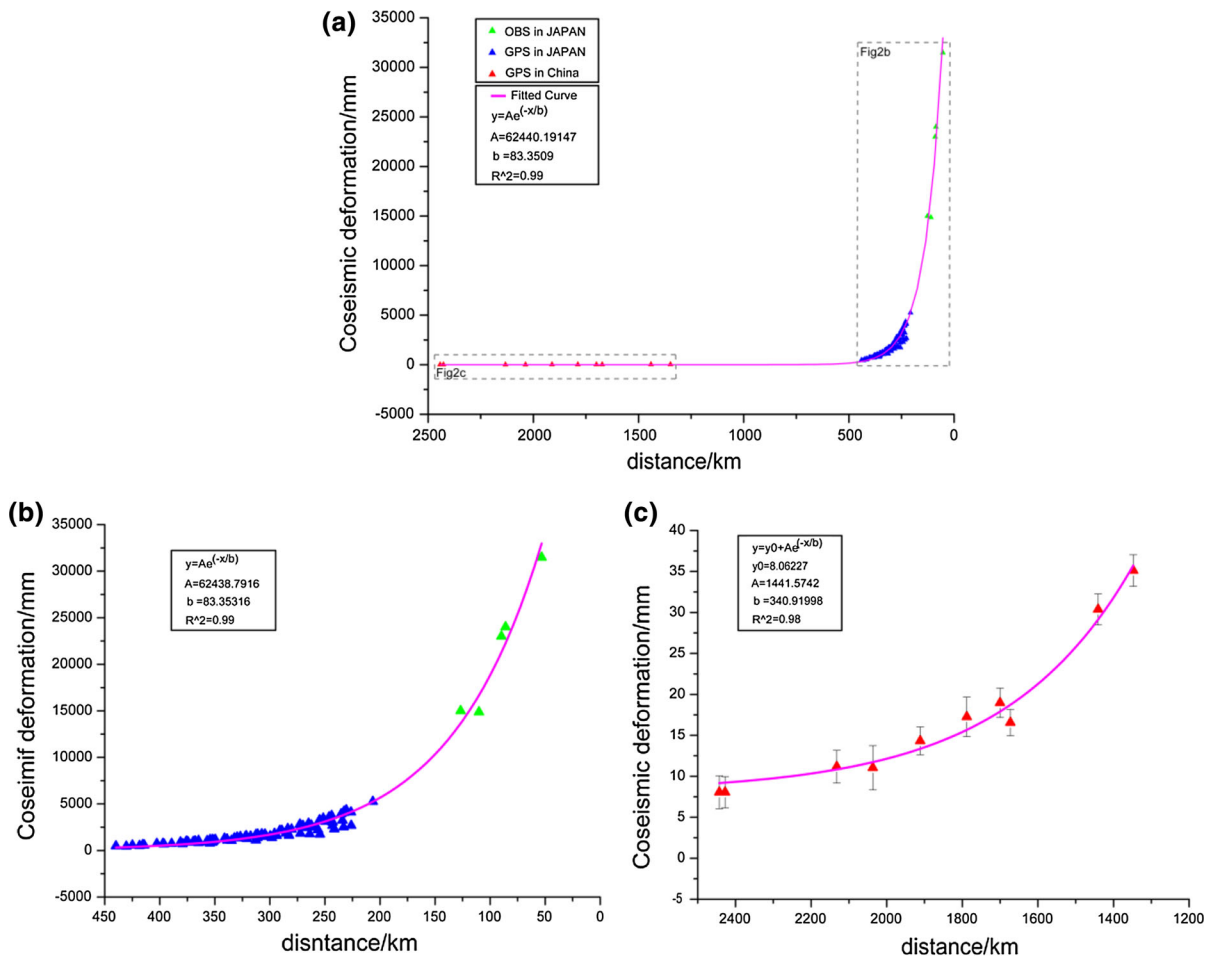
Figure 2

The relationship between the co-seismic displacement and the epicentral distance. **a** The observed co-seismic crustal deformation in the region denoted by the *dashed box* of Fig. 1; the *green triangles* are the co-seismic seafloor deformations above the fault, the *blue triangles* are the near-field crustal co-seismic deformations observed using near-field GPS on the Japanese Island, and the *red triangles* are the crustal displacements observed by far-field GPS in mainland China and the Korean Peninsula. **b** The value of the near-field crustal co-seismic displacement follows an exponential decay trend with distance from the epicenter. **c** The far-field co-seismic displacements (i.e., those more than 1000 km away from the focus) also decay exponentially with epicentral distance

2011). However, the results of these methods are in disagreement; for example, the maximum dislocations in some results are nearly 60 m (Fig. 3b, SHAO *et al.* 2011), while they are derived to be just over 30 m in other studies (Fig. 3c, WEI *et al.* 2011). ZHOU *et al.* (2012) found significant differences between the theoretical results and the near-field measurements using different models, but only small differences in the far-field data. Thus, Zhou et al. believe significant differences would not occur in the far field because of the varying co-seismic

dislocations. In this article, we also note the same phenomenon (Fig. 3a), but this does not mean that the co-seismic dislocation has little influence on the far-field co-seismic displacement. We observed that the spatial distributions given by the two co-seismic dislocation models mentioned above were consistent, but the maximum dislocation varied greatly between magnitudes 9.0 and 9.1. Based on the dislocation model developed by SHAO *et al.* (2011), we analyzed the relationship between the moment magnitude and the far-field co-seismic displacement fitting residuals.
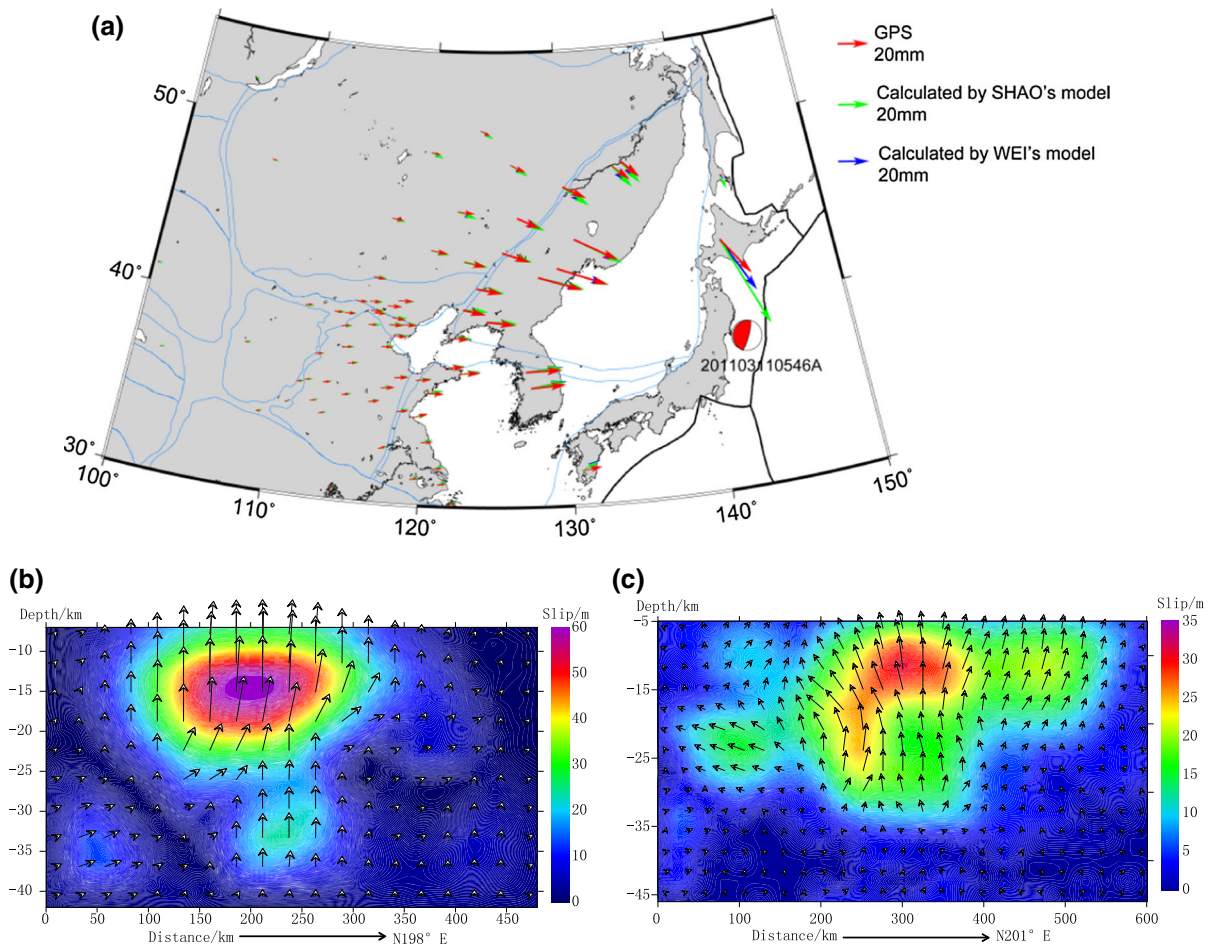
Figure 3

a The spatial distribution of the far-field co-seismic displacement observations (*red arrows*) and the simulation values (*green* and *blue arrows*). The *green arrows* are theoretical values of the far-field co-seismic displacements, calculated using the co-seismic dislocation model in **b** referred by SHAO *et al.* (2011); the *blue arrows* indicate the values from the co-seismic dislocation model in **c** obtained through the inversion method of WEI *et al.* (2011)

In this article, we varied the value of the dislocation by percentage instead of varying the spatial distribution of the dislocations. This work also uses the error function from ZHOU *et al.* (2012).

Figure 4a shows the relationship between the co-seismic moment magnitude and the displacement error, defined here as the difference between the theoretical values of the far-field displacements and their actual values observed using GPS on the Chinese mainland. The figure shows that the moment magnitude of this Tohoku-Oki earthquake was most likely M_W 9.06 using far-field co-seismic displacements more than 1000 km from the focus. Although

there is little difference in the error caused by an M_W 9.0 earthquake or an M_W 9.1 earthquake, the GPS data indicated that the actual far-field co-seismic displacement was smaller than the calculated displacement for a M_W 9.1 earthquake, and larger than that of a M_W 9.0 earthquake. That is, the GPS data indicate that the far-field co-seismic displacement was very sensitive to the magnitude of this Tohoku-Oki earthquake.

Both the moment magnitude and the maximum dislocation were relatively small if only the GPS-observed near-field co-seismic displacement data are used as a constraint (DIAO *et al.* 2011). This may be a
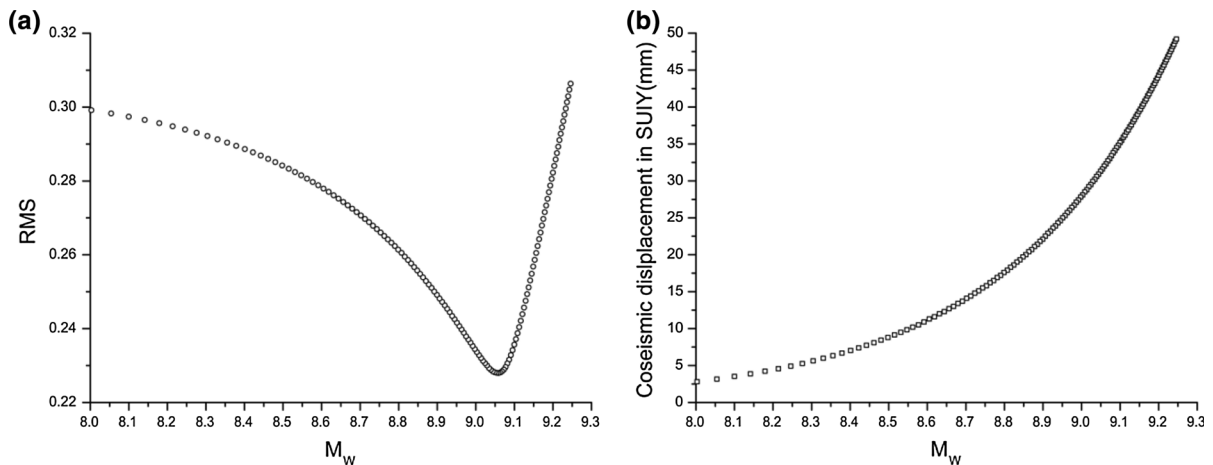
Figure 4
a The relationship between displacement error (defined in text) and the value of the magnitude. **b** Co-seismic displacement measured at SUIY station (China) caused by earthquakes of varying magnitude in the Japan Trench region. RMS is obtainable using the formula (1). The RMS misfit *curve* shows a clear unique global minimum at Mw 9.06

result of each near-field GPS measurement point only being sensitive to parts of the co-seismic dislocation. Therefore, an unfavorable distribution of near-field GPS stations may have offset the advantage offered by the numerous data points. However, while far-field GPS observations are not sensitive to the spatial distribution of the co-seismic dislocation, they are sensitive to the energy released by the event. We also calculated the theoretical co-seismic displacements at the SUIY GPS station in China caused by different magnitude events occurring in the Japan Trench region. We found that a significant co-seismic displacement can be detected on the Chinese mainland when an earthquake with a magnitude over 8.0 occurs in the Japan Trench (Fig. 4b).

3. Post-seismic Far-Field Response Following the March 11, 2011 Tohoku-Oki Earthquake

3.1. Previous Studies on the Near-Field Post-seismic Deformation

The 11th March M_W 9.0 earthquake in the Japan Trench was similar to other strong earthquakes, such as the M_W 9.5 Chile earthquake in 1960, in that it exhibited an obvious post-seismic displacement in

addition to significant near-field co-seismic displacements (LORENZO *et al.* 2006; OZAWA *et al.* 2011, 2012). Based on the GPS-based post-seismic crustal deformation data from Japan GEONET, DIAO *et al.* (2013) analyzed the temporal and spatial evolution of the aseismic fault slip near the Japan Trench after the earthquake. The same authors also estimated the effective viscosity coefficient of the upper mantle along the Japan Trench subduction, which can be used to explain the post-seismic crustal deformation observations in Japan. These previous results were based on the near-field geodetic observations.

Omori's law has been used to fit the aftershock occurrence rate (UTSU 1961), and, recently, it has been widely applied to afterslips (WENNERBERG and SHARP 1997; MONTÉSI 2004; LANGBEIN *et al.* 2006; HELMSTETTER and SHAW 2009). Figure 5a shows the cumulative moment released by the afterslip of the M_W 9.0 Tohoku-Oki earthquake as a function of time. We apply a modified form of Omori's law to fit this cumulative moment as

$$M = \frac{M_0 t^* \left[(1 + t/t^*)^{1-p} - 1 \right]}{1 - p} + M_1 t, \qquad (1)$$

where M is cumulative moment, t is the time since main shock (days); t^*, M_0, M_1, and p are fitting
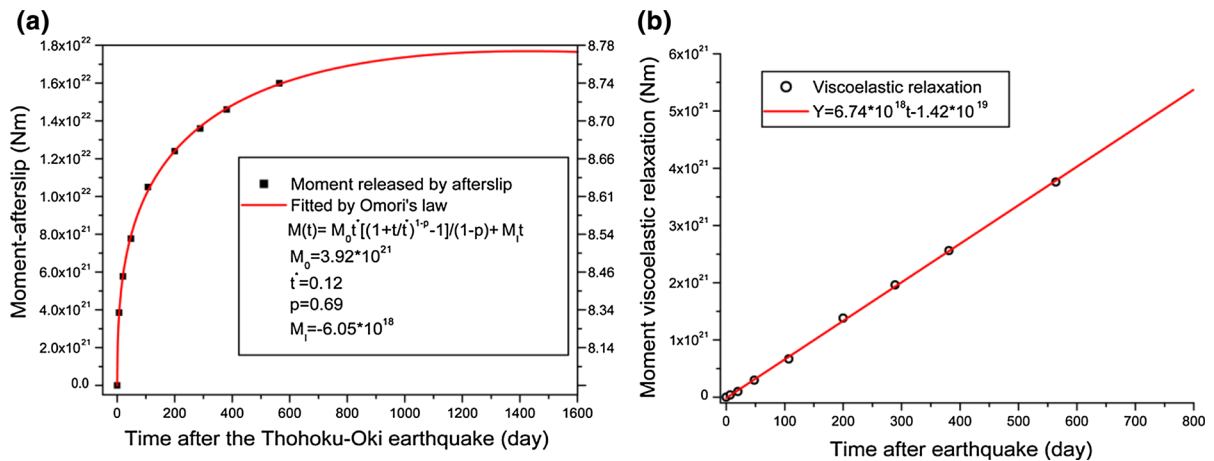
Figure 5
The cumulative moment released by the postseismic effect. **a** The afterslip of the March 11th Tohoku-Oki earthquake over time (DIAO *et al.* 2013), and **b** is the cumulative moment corresponding to the surface deformation caused by post-seismic viscoelastic relaxation varies in time (DIAO *et al.* 2013)

parameters, t^* is characteristic time, M_0 is initial value, M_1 is a constant changing rate, and p is exponent of energy rate decay. The value of p obtained from the fit is approximately 0.69. Based on this fitting formula, we extrapolated the gradient of the aseismic fault slip with time variation and determined that it will decrease to zero after 3.9 years following this earthquake (Fig. 5a); the total moment released by the afterslip is equivalent to that of a M_W 8.77 earthquake. DIAO *et al.* (2013) found that the relative proportion of the crustal deformation caused by the viscoelastic relaxation in the post-seismic deformation increased with time after the event. Using an inversion method with the post-seismic GPS crustal deformation data from Japan, they estimated the optimal values of elastic crust thickness and lithosphere viscosity to be 40 km and 8×10^{18} Pa s, respectively, both of which are close to the inversion results from the post-seismic crustal deformation data after the Hokkaido Nansei-Oki M_W 7.8 earthquake in 1993 (UEDA *et al.* 2003). We simulated the post-seismic crustal deformations caused by viscoelastic relaxation and found that for short time scales, the change was linear (Fig. 5b). The annual crustal deformation caused by the viscoelastic relaxation is equivalent to the co-seismic deformation caused by an M_W 8.02 earthquake.

3.2. GPS Observations and Theoretical Simulations of Post-seismic Crustal Deformation

To compare the far-field crustal deformation changes before and after the shock on the Chinese mainland and the Korean Peninsula, we selected 13 GPS continuous observation stations that had been in operation for over 4 years before the M_W 9.0 Tohoku-Oki earthquake, and subsequently obtained the single-day solution processed by GAMIT/GLOBK 10.40. The analysis process is as follows: (1) calculate the linear trend of the time series before March 11th, 2011 (Fig. 6a); (2) subtract the pre-earthquake linear trend from the time series after March 11th, 2011 (Fig. 6b); (3) subtract the co-seismic step from the post-seismic time series and obtain time-varying post-seismic far-field crustal deformation (Fig. 6c); (4) calculate the post-seismic far-field displacement caused by the afterslip and the viscoelastic relaxation following the M_W 9.0 Tohoku-Oki earthquake, and subsequently fit the data using the modified Omori's law given in Eq. (2) (Fig. 6c), and (5) subtract the simulated co- and post-seismic far-field effect from the initial time series to obtain the residual data showing the continuation of the pre-seismic linear trend as shown in Fig. 6d.

The formula used to fit the post-seismic displacement using the modified Omori's law is (HELMSTETTER and SHAW 2009)
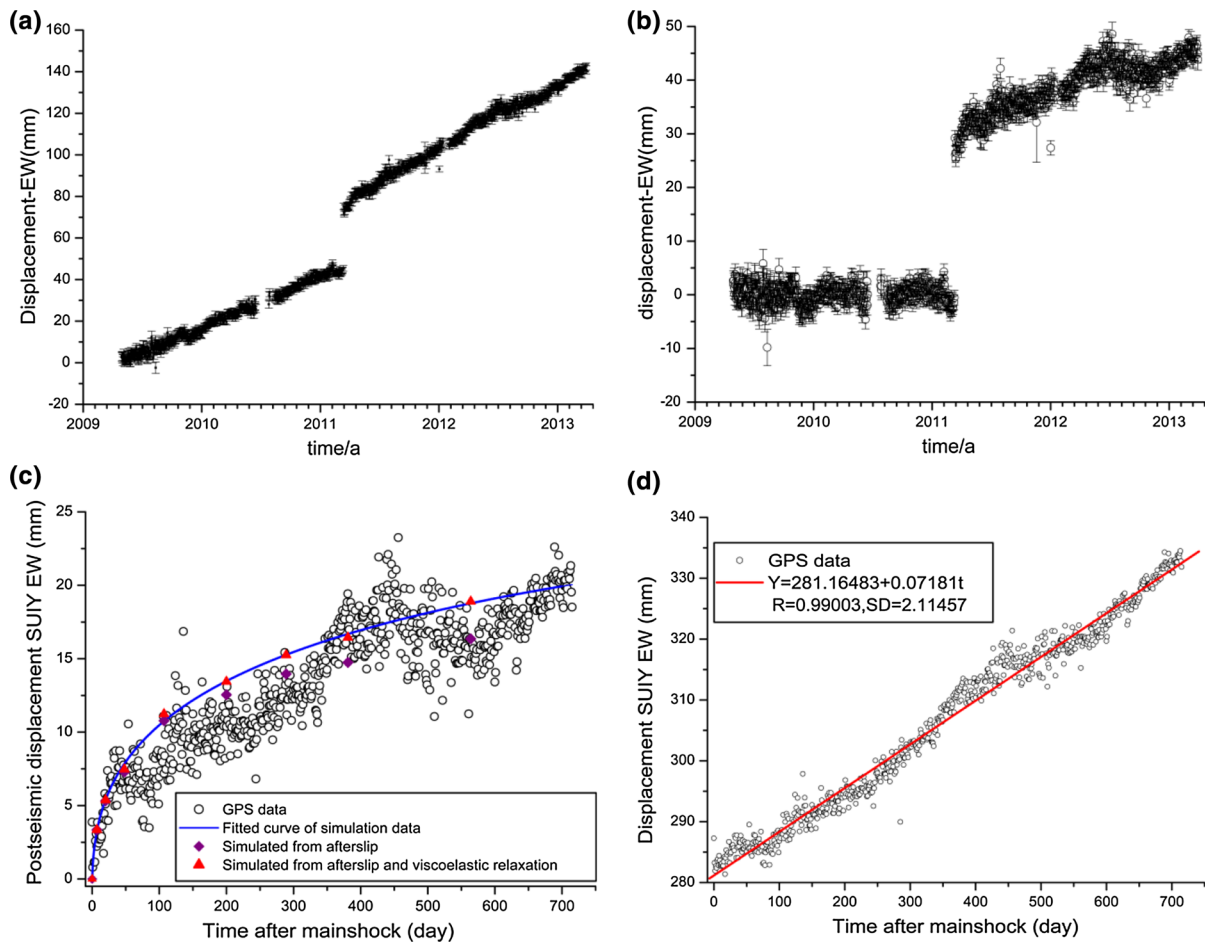
Figure 6
The analysis process for the GPS observation data from the SUIY station. **a** The time-series data observed at the station; **b** the data with the pre-earthquake linear trend subtracted from the time-series data; **c** the data with the pre-earthquake linear trend and the co-seismic step of the Tohoku-Oki 9.0 earthquake subtracted from the time-series data; **d** is obtained by subtracting the post-seismic changes caused by the afterslip and the viscoelastic relaxation of the March 11 event from the post-seismic observations in the time-series data

$$V = \frac{V_0 t^* \left[(1 + t/t^*)^{1-p} - 1 \right]}{1 - p} + V_l t, \qquad (2)$$

where V is post-seismic displacement, t is the time since main shock (days); t^*, V_0, V_l, and p are fitting parameters, t^* is characteristic time, V_0 is initial value, V_l is a constant changing rate, and p is exponent of displacement rate decay. The fitting parameters of the theoretical post-seismic displacements at the various stations are shown in Table 1. There are a number of differences in the p values among the stations, but, as a whole, they are close to the p value of the cumulative energy released by the

afterslip, and the values in the east–west direction are smaller than those in the north–south direction.

Figure 7 shows the post-seismic crustal displacement observed on the Chinese mainland and the Korean Peninsula during the first 1.5 years after the M_W 9.0 Tohoku-Oki earthquake. The GPS data indicate that the far-field post-seismic displacement within a year and a half of this earthquake is consistent with the far-field crustal deformations caused by the afterslip and the viscoelastic relaxation. In other words, the far-field post-seismic effect of the M_W 9.0 earthquake can be explained largely by the afterslip and the viscoelastic relaxation. The GPS

Table 1

Fitting parameters for the observed and calculated post-seismic far-field displacements

Station	GPS/mm	SIM/mm	V_0	t^*	p	V_1
BJSH						
EW	3.58	4.82	0.6971	0.2073	0.6571	−2.03E−03
NS	0.27	0.12	0.5635	0.0133	0.8764	−6.94E−05
CHUN						
EW	8.42	11.79	1.0527	0.4435	0.6694	−3.36E−03
NS	−4.67	−4.22	−0.1452	2.2379	0.7298	−3.76E−05
DAEJ						
EW	16.93	14.67	4.3059	0.0439	0.6285	−3.63E−03
NS	6.32	3.01	37.1336	2.85E−04	0.6905	5.43E−06
HLAR						
EW	2.78	4.10	0.3055	0.6629	0.6643	−2.03E−03
NS	−1.28	−2.05	−0.0831	1.9103	0.7114	4.60E−04
HRBN						
EW	10.42	10.21	0.8237	0.5140	0.6610	−3.59E−03
NS	−4.38	−5.66	−0.2224	1.7252	0.7062	4.38E−04
JIXN						
EW	8.79	5.45	0.7712	0.2110	0.6564	−2.21E−03
NS	−1.10	0.11	0.1597	0.1164	1.0086	−6.56E−05
KHAJ						
EW	4.09	4.63	0.2365	1.2023	0.6232	−4.10E−03
NS	−9.66	−8.66	−0.2004	5.4519	0.7643	1.09E−03
SUIY						
EW	19.73	18.92	1.5797	0.4307	0.6552	−4.79E−03
NS	−14.60	−12.79	−0.4696	1.7552	0.7082	−4.48E−04
SUWN						
EW	18.74	15.74	3.3331	0.0799	0.6363	−3.64E−03
NS	4.74	2.05	9.0595	2.39E−03	0.7390	8.41E−05
TAIN						
EW	3.51	4.32	0.9737	0.0964	0.6498	−1.84E−03
NS	2.85	0.91	1.1137	8.14E−03	0.6673	−3.19E−04
SHAO						
EW	3.12	3.23	4.9201	4.24E−03	0.6403	−1.38E−03
NS	3.90	1.60	5.88E+5	2.18E−11	0.6494	−4.50E−04
ZHNZ						
EW	3.67	2.72	0.7066	0.0818	0.6525	1.28E−03
NS	2.51	0.78	0.6796	0.0130	0.6601	−3.10E−04
WUHN						
EW	3.90	2.02	1.0253	0.0287	0.6524	−9.58E−04
NS	1.80	0.90	2.0196	2.81E−03	0.6553	−3.44E−04

data also indicate that the post-seismic displacement after this earthquake at the SUIY station was 24.6 mm (Table 1) and that the co-seismic displacement was 31.8 mm. Compared with the results of WANG *et al.* (2001) that the crustal deformation of the northeastern China mainland relative to the Eurasian frame is <5 mm/year, the far-field post-seismic crustal deformation following the 9.0 earthquake is significant.

4. Coulomb Failure Stress Changes in the Far Field

The stress field obtained by the focal mechanism solutions indicates that there were significant variations in the regional stress near the Japan Trench before and after the M_W 9.0 Tohoku-Oki earthquake (HASEGAWA *et al.* 2012), which changed the Coulomb stress not only in the subduction zone (YE *et al.* 2012) but also in the tensional fault east of the subduction
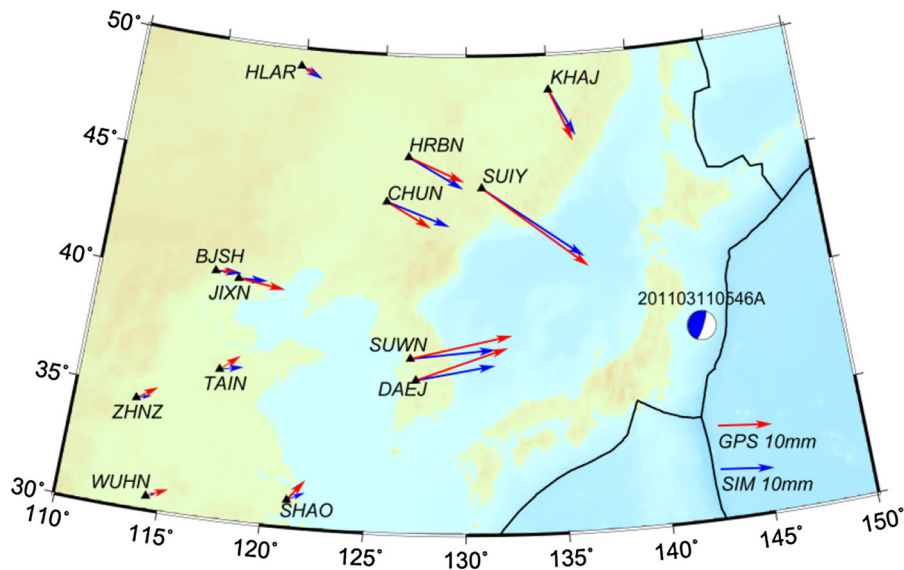
Figure 7

The far-field post-seismic crustal displacement within 1.5 years of the March 11th Tohoku-Oki earthquake. The *red arrows* are the GPS observations, and the *blue arrows* are the far-field post-seismic crustal displacement caused by the afterslip and the viscoelastic relaxation

zone (TODA *et al.* 2011; HIRATSUKA and SATO 2011). The most commonly used method to analyze the influence of earthquakes on stress accumulation in a fault involves determining the Coulomb stress changes (HARRIS 1998), where the formula for the Coulomb stress change is

$$\Delta\sigma_f = \Delta\tau + \mu'\Delta\sigma_n. \qquad (3)$$

In this equation, τ is the shear stress, σ_n is the normal stress, and μ' is the effective coefficient of friction.

In this section, we analyze the Coulomb stress changes induced by the 9.0 Tohoku-Oki earthquake on the main faults in northeast and northern China. There are a large number of faults in these two areas as shown in Fig. 8. The parameters of these faults mainly refer to the existing earthquake focal mechanisms (JIANG *et al.* 2011) and are based on the results of a number of field studies (DENG *et al.* 2003). These faults can be divided into three types according to strike: NE-trending, NW-trending, and approximately EW-trending. The co-seismic Coulomb stress was enhanced after the M_W 9.0 earthquake in most of the NE-trending faults, while

it weakened in NW-trending, EW-trending, and a small number of NE-trending faults (Fig. 8a). The Coulomb stress changes induced by the afterslip were slightly less but still close to the changes caused by the co-seismic effect (Fig. 8b), and the Coulomb stress changes induced by the viscoelastic relaxation within 10 years will be similar to the changes caused by the co-seismic effect (Fig. 8c). These independent effects mentioned above do not approach the stress triggering threshold; however, the cumulative Coulomb stress changes induced by co-seismic effects, afterslip, and viscoelastic relaxation within 10 years will probably exceed the trigger threshold at a few faults (Fig. 8d). Among these faults, the Yilan-Yitong fault and the Dunhua-Mishan fault of the northern section of the Tan-Lu fault zone show the greatest increases in stress, with the Yalujiang and the Fuyu-Zhaodong faults also showing significant stress increases. Most of the $M_L \geq 4.5$ seismicity after the M_W 9.0 earthquake was associated with the NE-trending faults, but the Yilan-Yitong, Dunhua-Mishan, Yalujiang, and Fuyu-Zhaodong faults were not among them. While a number of field studies show this, the Yilan-Yitong
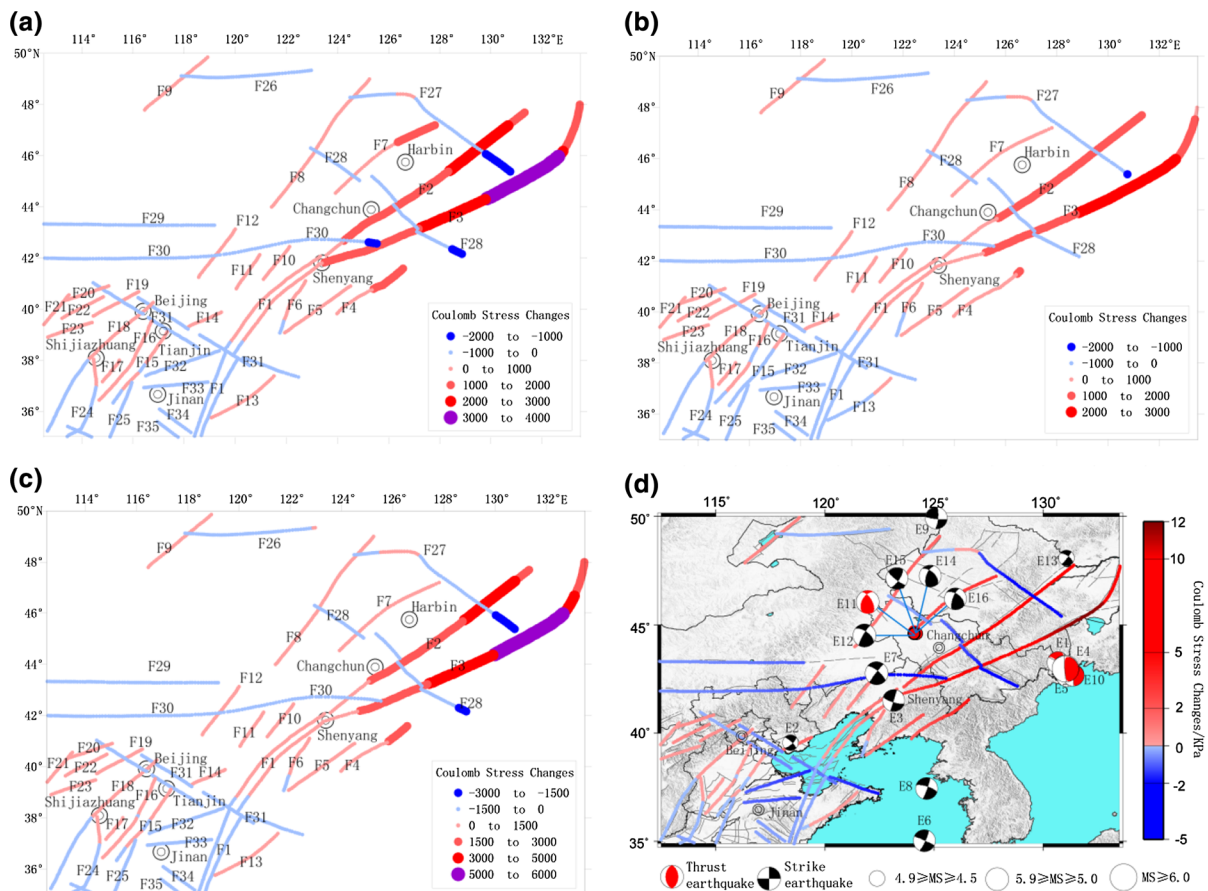
Figure 8

Coulomb stress changes (Pa) on the main faults in northeast and northern China caused by the March 11th Tohoku-Oki earthquake. **a** The Coulomb stress changes caused by the co-seismic effect; **b** Coulomb stress changes caused by afterslip; **c** Coulomb stress changes caused by viscoelastic relaxation projected to occur within 10 years after the event; and **d** the cumulative Coulomb stress changes induced by the co-seismic, afterslip, and the viscoelastic relaxation effects expected within 10 years. The *black circles* indicate the $M_L \geq 4.5$ events that have occurred in these regions since March 11th, 2011 (from the China Earthquake Networks Center). The fault zones are as follows: F1 Tan-Lu fault zone, F2 Yilan-Yitong fault zone, F3 Dunhua-Mishan fault zone, F4 Yalujiang fault zone, F5 Zhuanghe fault zone, F6 Jinzhou fault zone, F7 Fuyu-Zhaodong fault zone, F8 Nenjiang fault zone, F9 Hulunhu fault, F10 Jinzhou-Fuxin fault zone, F11 Beipiao-Chaoyang fault zone, F12 Balihan fault zone, F13 Haiyang fault zone, F14 Ninghe-Changli fault zone, F15 Chengxi fault zone, F16 Cangdong fault zone, F17 Xinhe fault zone, F18 Taihang mountains fault zone, F19 southern marginal fault zone of the Yuxian basin, F20 northern marginal fault zone of Tianzhen-Yanggao, F21 Kouquan fault zone, F22 northern foot fault zone of the Liuleng mountain, F23 northern foot fault zone of the Wutai mountain, F24 piedmont fault zone of the Taihang mountains, F25 Liaocheng-Lankao fault zone, F26 Hailaer fault zone, F27 Namohe-Boli-Beian fault zone, F28 the second Songhua river fault zone, F29 Xilamulun fault zone, F30 Kaiyuan-Chifeng fault zone, F31 Zhangjiakou-Bohai seismic belt, F32 Lingxian-Xinyang fault zone, F33 Guangji fault zone, F34 piedmont fault zone of Mengshan, and F35 Cangni fault zone (Deng *et al.* 2003 ; Institute of Geology 1987; Zhang *et al.* 2003)

fault was active during the Holocene period with an $M \geq 7$ earthquake 1730 ± 40 years ago (Min *et al.* 2011), and $M \geq 6$ earthquakes have occurred in the southwestern region of the Yalujiang fault, such as the M 6.1 earthquake in 1917 and the M 6.8 earthquake in 1944 (Earthquake Damage Prevention Department 1995).

5. Discussion of Crustal Strain in Northeast and Northern China

The M_W 9.0 Tohoku-Oki earthquake caused a very significant far-field co-seismic and post-seismic response. What is noteworthy was that the co-seismic response was instantaneous, and the duration of

afterslip was not very long, but the contributions of the post-seismic viscoelastic relaxation induced by this significant earthquake will last a long time. For example, a significant crustal deformation caused by the viscoelastic relaxation from the M_W 9.5 Chile earthquake in 1960 can still be detected 30 years later (Lorenzo et al. 2006; Klotz et al. 2001). Based on the viscoelastic medium model, we calculated the theoretical post-seismic crustal deformation. The results show that the crustal deformation subsequent to the earthquake follows an exponential decay trend above the epicenter and that the major post-seismic deformation will occur during the first 100 years

following the earthquake (Fig. 9a). At the SUIY station, which is 1276 km away from the epicenter, although the post-seismic crustal deformation decays exponentially with time as a whole, a linear variation is found for the first 200 years following the earthquake (Fig. 9b). In addition, at the SUIY station, the viscoelastic relaxation will induce crustal velocity changes of 2.75 mm/a for a significant period of time subsequent to the March 11 Tohoku-Oki earthquake, which means that the post-seismic displacement from viscoelastic relaxation in 11.56 years may be equivalent to the co-seismic displacement of this 9.0 earthquake (Fig. 9c).
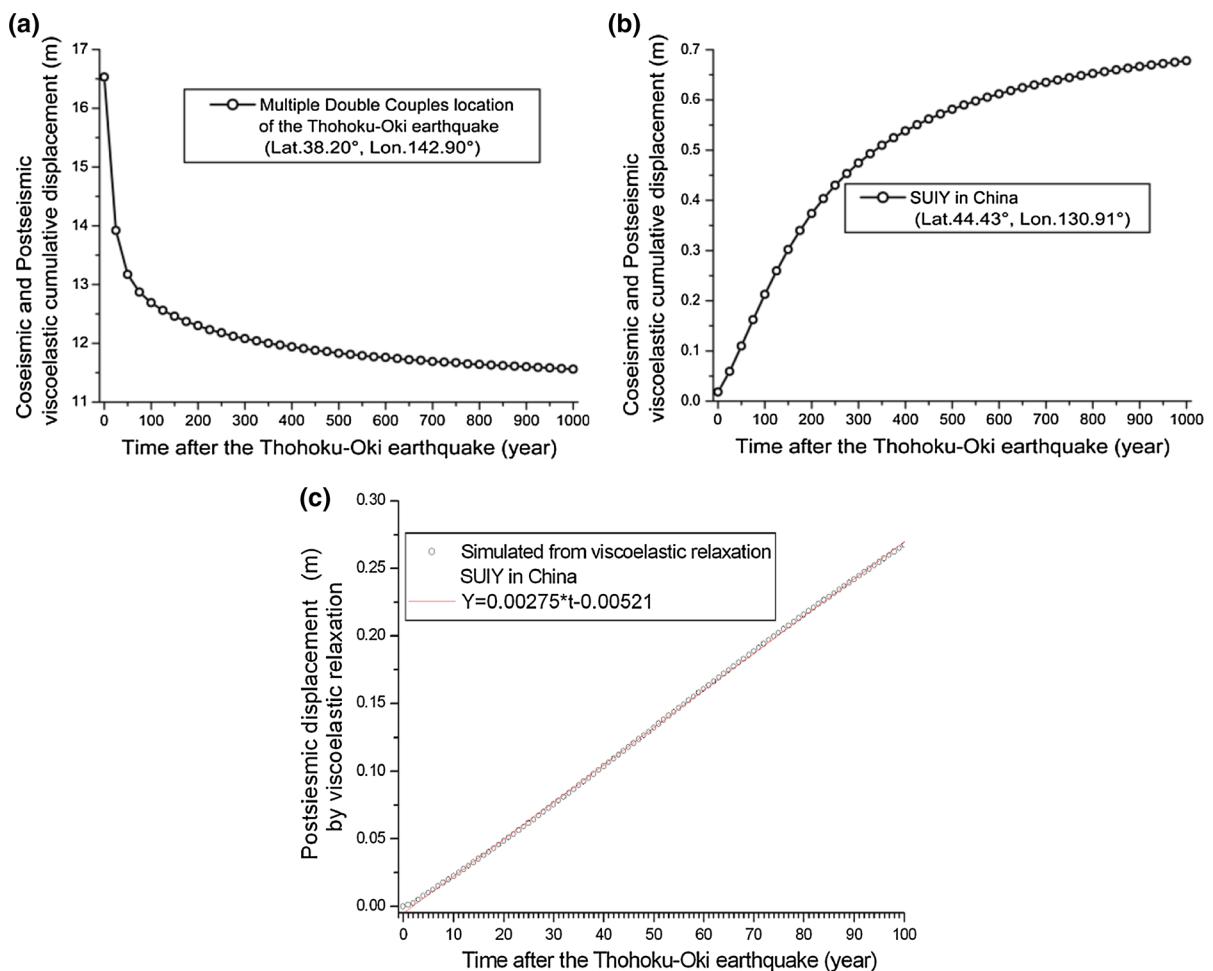

Figure 9
Crustal deformation subsequent to the earthquake. **a** The crustal deformation subsequent to the earthquake above the epicenter; **b** the coseismic and post-seismic viscoelastic cumulative displacement at the SUIY station; **c** the post-seismic displacement changes over time at the SUIY station caused by the viscoelastic relaxation of the March 11th 2011 Tohoku-Oki earthquake

A number of studies show that the evolution of important geological structure belts in northeast and northern China is inseparable from the subduction of the Pacific plate. The Tan-Lu fault, the largest fault in this region, is a good example. In the early Cretaceous period, the Izanagi plate obliquely subducted below East Asia with a high speed, most likely caused by the Pacific super-plume (MARUYAMA et al. 1997), and it may be the dynamic source for the sinistral strike-slip of the Tan-Lu fault. During the late Cretaceous, the Izanagi plate moved northward, while at the same time, the Pacific plate subducted at a medium-speed at the margin of the Chinese mainland (MARUYAMA et al. 1997), and the subduction angle changed from 10° to 80° (ZHOU and LI 2000). A high-angle forward subduction resulted in the asthenosphere upwelling and the lithosphere delamination in northern China. In this process, large extensional tectonics appeared on the strike-slip tectonics, with extension activity occurring earlier in the south than in the north (ZHU et al. 2001). Since the Neogene period, the subduction direction of the Pacific plate has changed from NNW to NWW, and, simultaneously, the Indian plate moved toward the NE. Thus, the Tan-Lu fault developed a thrust with a dextral strike-slip motion (ZHU et al. 2002).

The change of the westward subduction motion of the Pacific plate also induced the lithosphere upwelling in East Eurasia. This affected the geological structure and volcanic activity not only in East China, but also in Mongolia and southern Siberia (YIN 2010). Seismic tomography measurements (HUANG and ZHAO 2006) indicate that the westward subduction of the Pacific plate flattened at 660 km and extended into northeastern and northern China. It may have had a direct impact especially on deep earthquake and volcanic activity in northeast China. It should be noted that the Yilan-Yitong and Dunhua-Mishan faults were the regions of the Chinese mainland most affected by the 9.0 Tohoku-Oki earthquake.

The eastern boundary of the Amurian microplate is made up of the Japan Trench subduction zone, the Japan Nankai subduction zone, and the southwest subduction boundary of the Okhotsk block (APEL et al. 2006). Based on historical earthquake studies, large earthquakes have also occurred in the Japan Nankai trough (ISHIBASHI 2004; MOCHIZUKI and OBANA

2003). If such events with magnitudes similar to the March 11th Tohoku-Oki earthquake have occurred in either of the subduction zones mentioned above, then the effects of such powerful earthquakes should be taken into account during an analysis of the regional crustal deformation in northeastern and northern China. However, the method by which to account for these effects requires further studies and additional observations.

6. Conclusion

Continuous GPS observations of the significant far-field co-seismic and post-seismic displacements induced by the M_W 9.0 Tohoku-Oki earthquake on March 11th 2011 were performed. In this study, we made the following observations.

1. The far-field GPS-observed co-seismic displacement data are very sensitive to the magnitude of events similar to the M_W 9.0 Tohoku-Oki earthquake; Significant far-field co-seismic displacement can be observed in Eurasia only when the moment magnitude of the earthquake is greater than 8.0 near the Japan Trench.

2. The afterslip following the M_W 9.0 Tohoku-Oki earthquake decays exponentially with time and may come to an end 4 years after the event. The post-seismic crustal deformation will be mainly caused by viscoelastic relaxation. The post-seismic displacement within 1.5 years observed by GPS in Eurasia can be explained by the afterslip and the viscoelastic relaxation.

3. The co-seismic and post-seismic Coulomb stress caused by this earthquake was enhanced significantly in many NE-trending faults in northeastern and northern China, especially in the Yilan-Yitong and the Dunhua-Mishan faults (the northern section of the Tan-Lu fault zone), as well as the Yalujiang and Fuyu-Zhaodong faults.

4. The far-field post-seismic displacement in Eurasia caused by the viscoelastic relaxation within 10 years will be equivalent to the co-seismic displacement following the M_W 9.0 Tohoku-Oki earthquake. Thus, the post-seismic effect caused by the viscoelastic relaxation after such an

earthquake should not be ignored in regional deformation and dynamics studies.

REFERENCES

APEL, E.V., BÜRGMANN, R., STEBLOV, G., VASILENKO, N., KING, R., PRYTKOV, A., 2006. Independent active microplate tectonics of northeast Asia from GPS velocities and block modeling. Geophys. Res. Lett. *33*, L11303, doi:10.1029/2006GL026077.

CHEN, P. F., BINA, C. R., OKAL, E. A., 2004. A global survey of stress orientations in subducting slabs as revealed by intermediate-depth earthquakes. Geophys. J. Int. *159*, 721–733.

DENG, Q. D., ZHANG, P. Z., RAN, Y. K., YANG, X. P., MIN, W., CHEN, L. C., 2003. Active tectonics and earthquake activities in China. Earth Science Frontiers *10*(Suppl), 66–73 (in Chinese).

Department of Earthquake Monitoring and Prediction. China Earthquake Administration, 2007. Summary of the Asian Earthquake (in Chinese). Seismological Press.

DIAO, F.Q., XIONG, X., WANG, R.J., ZHENG, Y., WALTER, T. R., WENG, H. H., LI, J., 2013. Overlapping post-seismic deformation processes: afterslip and viscoelastic relaxation following the 2011 Mw 9.0 Tohoku (Japan) earthquake. Geophys. J. Int. *196*(1), 218–229, doi:10.1093/gji/ggt376.

DIAO, F.Q., XIONG, X., NI, S.D., ZHENG, Y., GE, C, 2011. Slip model for the 2011 MW9.0 Sendai (Japan) earthquake and its MW7.9 aftershock derived from GPS data. Chinese Sci Bull *56*, doi:10.1007/s11434-011-4643-4.

Earthquake Damage Prevention Department, State Seismological Bureau, 1995. Catalogue of historical strong earthquake in China. Seismological Press.

HARRIS, R., 1998. Introduction to special section: stress triggers, stress shadows, and implications for seismic hazard. J. Geophys. Res. *103*, 24347–24358.

HASEGAWA, A., YOSHIDA, K., ASANO, Y., OKADA, T., 2012. Change in stress field after the 2011 great Tohoku-Oki earthquake. Earth Planet. Sci. Lett. *355–356*, 231–243.

HAYES, G. P., 2011. Rapid source characterization of the 03-11-2011 MW9.0 off the Pacific Coast of Tohoku earthquake. Earth Planets Space *63*, 529–534, doi:10.5047/eps.2011.05.012.

HELMSTETTER, A. and SHAW, B.E., 2009. Afterslip and aftershocks in the rate-and-state friction law. J. Geophys. Res. *114*, B01308, doi:10.1029/2007JB005077.

HIRATSUKA S. and SATO T., 2011. Alteration of stress field brought about by the occurrence of the 2011 off the Pacific coast of Tohoku earthquake (MW9.0). Earth Planets Space *63*, 681–685, doi:10.5047/eps.2011.05.013.

HUANG, J.L., ZHAO, D.P., 2006. High-resolution mantle tomography of China and surrounding regions. J. Geophys. Res. *111*, B09305, doi:10.1029/2005JB004066.

HWANG, J.S., YUN, H.Z., HUANG, H., JUNG, T.J., LEE, D.H, WE, K.J., 2012. Thohoku-Oki earthquake's influence on the Asian plates and Korean geodetic network. Chines J. Geophys. (in Chinese with English abstract) *55*(6), 1884–1893, doi:10.6038/j.issn.0001-5733.2012.

IINUMA, T, HINO, R, KIDO, M., INAZU, D., OSADA, Y., ITO, Y., OHZONA, M., TSUSHIMA, H., SUZUKI, S., FUJIMOTO, H., MIURA, S, 2012. Coseismic slip distribution of the 2011 off the Pacific Coast of Tohoku Earthquake (M9.0) refined by means of seafloor geodetic data. J. Geophys. Res. *117*, B07409, doi:10.1029/2012JB009186.

ISHIBASHI, K., 2004. Status of historical seismology in Japan. Ann. Geophys. *47*, 339–368.

INSTITUTE OF GEOLOGY, 1987. State Seismological Bureau, The Tan-Lu fault zone. Seismologicla Press (in Chinese).

JIANG, M.M., ZHOU, S.Y., CHEN, Y.J., AI, Y.S., 2011. A new multidimensional stress release statistical model based on coseismic stress transfer. Geophys. J. Int. *187*, 1479–1494, doi:10.1111/j.1365-246X.2011.05208.x.

KANAMORI, H, MIYAZAWA, M, MORI, J., 2006. Investigation of the earthquake sequence off Miyagi prefecture with historical seismograms. Earth Planets Space *58*, 1533–1541.

KANAMORI, H., 1977. Seismic and aseismic slip along subduction zones and their tectonic implications. In Island Arcs, Deep Sea Trenches and Back Arc Basins (eds. M Talwani & W C Pitman III), American Geophysical Union, 163–174.

KIDO, M., OSADA, Y., FUJIMOTO, H., Ito, Y., 2011. Trench-normal variation in observed seafloor displacements associated with the 2011 Tohoku-Oki earthquake. Geophys. Res. Lett. *38*, L24303, doi:10.1029/2011GL050057.

KLOTZ, J., KHAZARADZE, G., ANGERMANN, D., REIGBER, C., PERDOMO, R., CIFFUENTES, O., 2001. Earthquake cycle dominates contemporary crustal deformation in Central and Southern Andes. Earth Planet. Sci. Lett. *193*, 437–446.

KOPER, K. D., HUTKO, A. R., LAY, T., AMMON C. J., KANAMORI, H., 2011. Frequency-dependent rupture of the 11 March 2011 MW9.0 Tohoku earthquake: Comparison of short-period P wave back projection images and broadband seismic rupture model. Earth Planets Space *63*, 599–602, doi:10.5047/eps.2011.05.026.

LANGBEIN, J., MURRAY, J.R., SNYDER, H.A., 2006. Coseismic and initial postseismic deformation from the 2004 Parkfield, California, earthquake, observed by global positioning system, electronic distance meter, creepmeters, and borehole stranimeters. Bull. Seismol. Soc. Am. *96*, S304–S320.

LAY, T., AMMON, C. J., KANAMORI, H., XUE, L., KIM, M. J., 2011. Possible large near-trench slip during the great 2011 Tohoku (MW9.0) earthquake. Earth Planets Space *63*, 687–692, doi:10.5047/eps.2011.05.033.

LORENZO, M.F., ROTH, F., WANG, R.J., 2006. Inversion for rheological parameters from post-seismic surface deformation associated with the 1960 Valdivia earthquake, Chile. Geophys. J. Int. *164*, 75–87.

MARUYAMA, S, ISOZAKI, Y, KIMURA, G., TERABAYASHI, M. C., 1997. Paleogeographic maps of the Japanese Islands: plate tectonic synthesis from 750 Ma to the present. Island Arc *6*, 121–142.

MIN, W., JIAO, D. C., ZHOU, B. G., SHENG, J., CHEN, T., 2011. The significance of discovery on Holocene activity on the Yilan-Yitong fault in northeast China. Seismology and Geology *33*(1), 141–150 (In Chinese with English abstract).

MOCHIZUKI, K. and OBANA, K., 2003. Seismic activities along the Nankai Trough. Bull. Earthq. Res. Inst. *78*, 185–195.

MONTÉSI, L.G.J., 2004. Controls of shear zone rheology and tectonic loading on postseismic creep. J. Geophys. Res. *109*, B10404, doi:10.1029/2003JB002925.

OZAWA, S., NISHIMURA, T., MUNEKANE, H., SUITO, H., KOBAYASHI, T., TOBITA, M., IMAKIIRE, T., 2012. Preceding, coseismic, and postseismic slip of the 2011 Tokoku earthquake, Japan. J. Geophys. Res., *117*, B07404, doi:10.1029/2011JB009120.

OZAWA, S., NISHIMURA, T., SUITO, H., TOMOKAZU, K., TOBITA, M., TETSURO, I., 2011. Coseismic and postseismic slip of the 2011 magnitude-9 Tohoku-Oki earthquake. Nature *475*, 373–377, doi:10.1038/nature10227.

POLLITZ, F.F., BÜRGMANN, R., BANERJEE, P., 2011. Geodetic slip model of the 2011 M9.0 Tohoku earthquake. Geophys. Res. Lett. *38*, L00G08, doi:10.1029/2011GL048632.

SATO, M., ISHIKAWA, T., UJIHARA, N., YOSHIDA, S., FUJITA, M., Mochizuki, M., Asada, A., 2011. Displacement above the hypocenter of the 2011 Tohoku-Oki earthquake. Science *332*(6036), 1395, doi:10.1126/science.1207401.

SHAO, G., LI, X., JI, C., MAEDA, T., 2011. Focal mechanism and slip history of 2011 Mw 9.1 off the Pacific coast of Tohoku earthquake, constrained with teleseismic body and surface waves. Earth Planets Space *63*(7), 559–564, doi:10.5047/eps.2011.06.028.

SHESTAKOV, N.V., TAKAHASHI T., OHZONO, M., PRYTKOV, A., S., BYKOV, V. G., GERASIMENKO, M. D., LUNEVA, M. N., GERASIMOV, G. N., KOLOMIETS, A. G., BORMOTOV, V. A., VASILENKO, N. F., BEAK, J., PARK, P., SEROV, M. A., 2012. Analysis of the far-field crustal displacements caused by the 2011 Great Tohoku earthquake inferred from continuous GPS observations. Tectonophysics *524–525*, 76–86, doi:10.1016/j.tecto.2011.12.019.

SIMONS, M., MINSON, S.E., SLADEN, A., ORTEGA, F., JIANG, J., OWEN, S.E., MENG, L., AMPUERO, J.-P., WEI, S., CHU, R. S., HELMBERGER D. V., KANAMORI, H., HETLAND, E., MOORE, A. W., WEBB, F. H., 2011. The 2011 magnitude 9.0 Tohoku-Oki earthquake: Mosaicking the megathrust from seconds to centuries. Science *332*, 1421–1425, doi:10.1126/scienc.1205731.

TAJIMA, F., MORI, J., KENNETT, B. L.N., 2013. A review of the 2011 Tohoku-Oki earthquake (MW 9.0): large-scale rupture across heterogeneous plate coupling. Tectonophysics *586*, 15–34.

TAIRA, A., 2001. Tectonic evolution of the Japanese island arc system. Annu. Rev. Earth Planet. Sci. *29*, 109–134.

TODA, S., STEIN, R.S., LIN, J., 2011. Widespread seismicity excitation throughout central Japan following the 2011 M = 9.0 Tohoku earthquake and its interpretation by Coulomb stress transfer. Geophys. Res. Let. *38*, L00G03, doi:10.1029/2011GL047834.

UEDA, H., OHTAKE, M., SATO, H., 2003. Postseismic crustal deformation following the 1993 Hokkaido Nansei-oki earthquake, northern Japan: evidence fro a low-viscosity zone in the uppermost mantle. J. Geophys. Res., *108*(B3), 2151, doi:10.1029/2002JB002067.

UTSU, T., 1961. A statistical study on the occurrence of aftershocks. Geophys. Mag. *30*, 521–605.

WANG, Q, ZHANG, P.Z., FREYMUELLER, T.J., BILHAM, R., LARSON, M.K., LAI, X.A., YOU, X.Z., NIU, Z.J., WU, J.C., LI, Y.X., LIU, J.N., YANG, Z.Q., CHEN, Q.Z., 2001. Present-Day crustal deformation in China constrained by global positioning system measurements. Science *294*, 574–577.

WANG, M., LI, Q., WANG, F., ZHANG, R., WANG, Y.Z., SHI, H.B., ZHANG, P.Z., SHEN, Z.K., 2011. Far-field coseismic displacements associated with the 2011 Tohoku-oki earthquake in Japan observed by Global Positioning System. Chinese Sci. Bull. *56*, doi:10.1007/s11434-011-4588-7.

WEI, S., SLADEN, A., and the ARIA GROUP, 2011. Updated result 3/11/2011(Mw 9.0), Tohoku-oki, Japan, report, Calif. Inst. of Technol., Pasadena. [Available at http://www.tectonics.caltech.edu/slip_history/2011_taiheiyo-oki/.]

WENNERBERG, L. and SHARP, R.V., 1997. Bulk friction modeling of afterslip and the modified Omori law. Tectonophysics *277*, 109–136.

YE, L.L., LAY, T., KANAMORI, H., 2012. The Snriku-Oki low-seismicity region on the northern margin of the great 2011 Tohoku-Oki earthquake rupture. J. Geophys. Res. *117*, B02305, doi:10.1029/2011JB008847.

YIN, A., 2010. Cenozoic tectonic evolution of Asia: a preliminary synthesis. Tectonophysics *488*, 293–325, doi:10.1016/j.tecto.2009.06.002.

ZHANG, P. Z., DENG, Q. D., ZHANG, G. M., MA, J., GAN, W. J., MIN, W., 2003. Active tectonic blocks and strong earthquakes in the continent of China. Science in China (Ser D) *46*(suppl), 13–24.

ZHAO, B., WANG, W., YANG, S.M., PENG, M.L., QIAO, X.J., Du, R.L., Nie, Z.S., 2012. Far field deformation analysis after the Mw9.0 Tohoku earthquake constrained by cGPS data. J. Seismol. *16*, 305–313, doi:10.1007/s10950-011-9271-6.

ZHOU, X., SUN, W.K., ZHAO, B., FU, G.Y., DONG, J., NIE, Z.S., 2012. Geodetic observations detecting coseismic displacements and gravity changes caused by the Mw = 9.0 Tohoku-Oki earthquake. J. Geophy. Res. *117*, B05408, doi:10.1029/2011JB008849.

ZHOU, X. M. and LI, X. W., 2000. Origin of Late Mesozoic igneous rocks in Southeastern China: implications for lithosphere subduction and underplating of mafic magmas. Tectonophysics *326*, 269–287.

ZHU, G., WANG, D. X., LIU, G. S., SONG, C. Z., XU, J. W., NIU, M. L., 2001. Extensional activities along the Tan-Lu fault zone and its geodynamic setting. Chinese Jour. Geol. *36*(3), 269–278 (In Chinese with English abstract).

ZHU, G., LIU, G. S., NIU, M. L., SONG, C. Z., WANG, D. X., 2002. Post-Eogene compressive activities on the Tan-Lu fault zone and their deep processes. Seismology and Geology *24*(2), 265–277 (In Chinese with English abstract).